Radio Beamsteering for a 2×5 Remote Radio Head Assisted by a Shared Wideband Etalon Cascade

Aina Val Martí, David Löschenbrand, Thomas Zemen, and Bernhard Schrenk
AIT Austrian Institute of Technology, Center for Digital Safety&Security / Security & Communication Technologies, 1210 Vienna, Austria.
Author e-mail address: aina.val-marti@ait.ac.at

Abstract: We demonstrate RF beamsteering through cascaded Gires-Tournois etalons, yielding a delay-tailored DWDM feed for a 2×5 antenna configuration. 64-QAM OFDM radio is transmitted under 32° beam deflection. We further show kHz carrier phase switching.

1. Introduction

One of the key-features for future radio access networks is beamforming in combination with multi-element antennas, which allow to improve the performance of wireless systems while avoiding interference at the same time – thus greatly contributing to boost capacity and data rate [1]. Beamsteering can be accomplished by means of a programmable true-time delay associated to each antenna element [2], ideally being applicable to a wide RF frequency range and at low loss. Optically assisted methods have been intensively researched by virtue of their broadband nature. Next to switched delays implemented on photonic integrated circuits [3], continuous delay settings build on wavelength-dependent dispersive media such as fiber [4] or linearly chirped Bragg gratings [5] or elements offering a tunable group delay at resonance, such as micro-ring resonators [6] or waveguide gratings [7]. However, the tuning mechanism can quickly become complex, and the supported RF signal bandwidth faces a limit.

In this work, we propose a method for photonic-assisted RF beamsteering based on a cascade of Gires-Tournois etalons, which contribute with a wideband periodic evolution in group delay dispersion along the ITU-T DWDM grid. We experimentally confirm that the received EVM of a 64-QAM OFDM radio adheres to the beam deflection of a phased-array 2×5 antenna configuration and demonstrate the support for fast beamsteering at 2 kHz.

2. Shared Etalon Cascade as a Shared RF Beamformer

Optically assisted RF beamsteering can be accomplished through a shared optical element with periodic evolution for its group delay dispersion, meaning that the change in group delay due to the optical frequency repeats itself for consecutive DWDM channels. Specifically, we employ a cascade of Gires-Tournois etalons [8] with optical thickness d and reflectance R for this purpose, which contribute with an all-pass behavior having a group delay spectrum given by $\tau_{gr}(\nu) = \sum 2d/c\ (1-R) / [1+R+2\sqrt{R}\cos(2\pi\nu\ 2d/c)]$.

This function yields a sawtooth-like evolution over the optical frequency ν. This periodic response is exploited by dedicating the delay-tailored DWDM channels to the antenna elements of the downlink RRHs (Fig. 1a), thus allowing an element-by-element setting for the RF carrier phase and, consequently, enabling RF beamsteering.

The colorless wideband nature of a centralized etalon cascade allows for cost-sharing of the beamformer among many antenna sites and supports the notion for lean RRHs. It further allows to compensate its optical loss at a network site where EDFA-based amplification can be techno-economically justified.

A characterization of the group delay dispersion for an EC device used in the present experiment is shown in Fig. 1b and 1c, together with the transmission of the arrayed waveguide grating (AWG) later used to demultiplex the DWDM feed for the antenna elements at the RRH. The group delay dispersion has a periodicity of 50 GHz and is

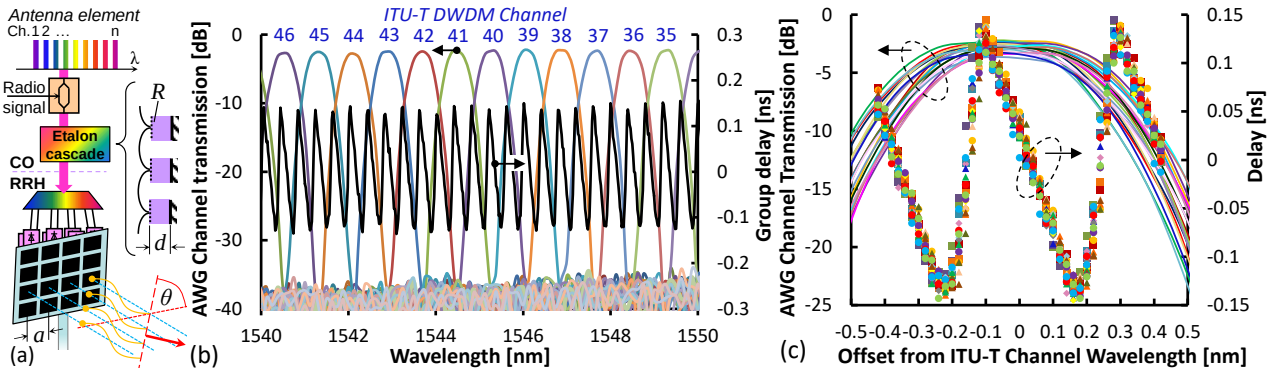

Fig. 1. (a) Photonic RF beamsteering method. AWG transmission and imposed group delay over (b) C-band channels and (c) relative to ITU-T center.

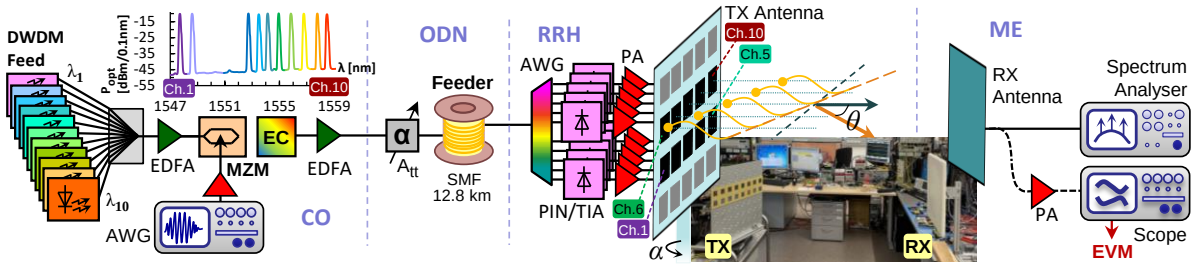

Fig. 2. (a) Experimental setup for a RF downlink with beamsteering. The photo inset shows the rotated TX antenna and fixed RX antenna.

centered to the nominal ITU-T channel wavelength. It ranges from -0.1 to 0.13 ns within the flat transmission region of a DWDM channel. This value is sufficiently high to accomplish beamsteering for a phased-array antenna configuration, even for a carrier frequency in the sub-6GHz wireless band.

3. Experimental Setup and Photonic-Assisted RF Beamsteering

The experimental setup is presented in Fig. 2. At the central office (CO), a DWDM comb with 10 wavelengths ranging from 1547.72 to 1558.17 nm are combined and jointly modulated with a Mach-Zehnder modulator (MZM) with the radio signal. The latter was a 64-QAM OFDM signal at 3.5 GHz, carrying 128 sub-carriers over 250 MHz. The comb is then processed by the cascade of Gires-Tournois etalons (EC) with a loss of 5.3 dB and further boosted by an EDFA to achieve a launch of 3 dBm/λ with an average OSNR of 36.7 dB/0.1nm. The optical distribution network (ODN) comprised of a variable attenuator (Att) to emulate a passive trunk split. It also sets the optical budget of the ODN. A 12.8-km long, ITU-T G.652B compatible single-mode fiber (SMF) was used as feeder.

At the RRH an AWG distributes the DWDM feed to the 2×5 antenna elements, for which the lower row was fed by Channels 1-5 and the upper row by Ch. 6-10. A 10G PIN/TIA receiver and an RF amplifier per element completes the RRH. As it can be seen in Fig. 2, the RRH as phased-array transmit antenna is arranged on a rotation platform (α) in order to evaluate the efficiency of beam steering. A directional receive antenna with a gain of 23 dB delivers the RF signal to the EVM and the received RF power analyses.

To evaluate the beamsteering, we imposed three different group delays between consecutive horizontal antenna elements through the EC, leading to relative phase shifts of φ = 0°, 74° and 150° at fRF = 3.5 GHz between these elements. The antenna elements in the same column (eg, Ch.3, 8) had the same relative phase, meaning that beam steering occurs in azimuth θ. Considering the well-known relation for the beam steering angle θ = arcsin(c δτ / a), where δτ is the delay and a is the distance between two antenna elements, the aforementioned phase shifts would theoretically correspond to beamsteering angles of θ = 0°, 20° and 44°, respectively. Figure 3 shows the RF carrier that was remotely fed from the CO to each of the antenna elements through the wavelength Ch. 1-10. The introduced RF carrier phase shift φ can be noticed. Figure 3 further includes the beam profile, which was obtained by rotating the TX antenna by an angle α while acquiring the received RF power at the stationary RX antenna. With equal group delay setting among all antenna elements (φ = 0), the main lobe points towards θ = -1° (○), meaning that the maximum power is received when the two antenna point towards each other. For φ = 74°, the steering angle θ becomes 15° (☆), and for φ = 150°, the TX antenna needs to be rotated by α = 32° (□) to see a maximum RF power transmission. The error in θ between theory and experiment, and the slight widening of the main lobe for an increased θ motivates the monitoring of the RF phase at the RRH and the use of an anechoic chamber for a more precise acquisition of the beam profile in further investigations. However, we did not observe a degrading effect arising from the feeder fiber.

4. Transmission Performance and RF Carrier Phase Switching

The radio signal transmission performance is discussed in Fig. 4. The received RF spectrum just after photodetection at one of the RRH elements is spectrally flat (Fig. 4a) and yields an average EVM of 6.7% for an optical feed power of -8 dBm (Fig. 4b, ●). We did not observe any interference fringes after RF propagation between the TX and RX antennas (Fig. 4a) but noticed the phased-array

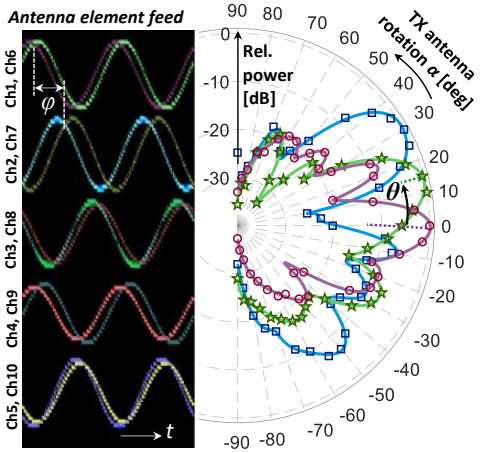

Fig. 3. Antenna element feeds for φ = 150° (□) and resulting beam steering for φ = 0° (○) and 74° (☆).

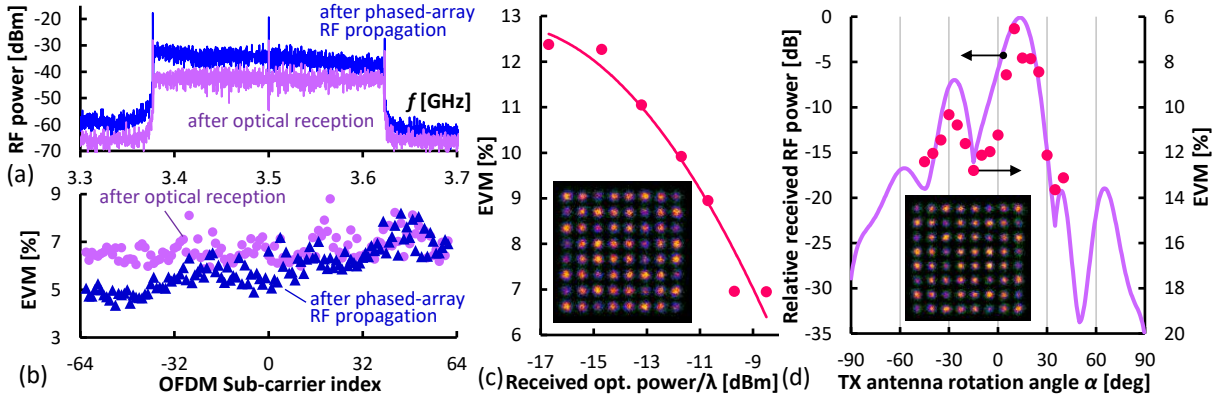

Fig. 4. (a) Received radio spectra and (b) EVM. (c) EVM as function of received optical power to the RRH. (d) EVM and RF power for $\theta = 15°$.

gain through a slightly improved EVM of 5.9% (Fig. 4b). The roll-off in RF power towards higher frequencies is attributed to fading inherent to RF propagation. This is also the cause for the slight rise in EVM with the OFDM sub-carrier index (▲).

Next, we investigated the EVM as function of received optical power per RRH antenna element (Fig. 4c). The EVM antenna limit of 8% for 64-QAM transmission is reached at an input level of -9.8 dBm/λ. The clean 64-QAM constellation for the 250-MHz wide OFDM transmission evidences the good transmission performance.

Moreover, we evaluated the EVM under a beamsteering angle of θ = 15° (corresponding to Fig. 3,☆). Figure 4d presents the EVM that has been overlaid to the received RF power, as function of the rotation angle α for the TX antenna. The EVM evolution over α matches that of the received RF power and shows a minimum for α = θ. Again, the received constellation for α = θ is clean.

Finally, the fast switching of the RF carrier phase at Ch. 1 has been accomplished through optical frequency modulation of the respective DFB laser source. Figure 5 shows the associated modulation of the DFB current Imod, skew-corrected to the received OFDM signal at the TX antenna element of Ch. 1. The switching frequency was 2 kHz and a gap of 50 µs has been inserted between two OFDM packets with relatively shifted RF carrier phase (φ1, φ2), in order to account for phase transitions errors. The received OFDM constellations, characterized by the position of the pilot tone π, reflect the optical frequency modulation imposed by the DFB through their relative alignment by Δφ = 7 and 35° for a peak-to-peak DFB modulation of Imod = 2 and 10 mApp, respectively. Though not applied to all antenna elements, it proves that the etalon cascade supports fast beamsteering.

5. Conclusion

We experimentally demonstrated an all-optical method for RF beamsteering in a RRH configuration with 2×5 antenna elements. The employed EC showed a periodic group delay dispersion, which not only adheres to the ITU-T DWDM grid but also enables the delay tuning on a per-element basis. The steered RF beam profiles agreed to the experimentally acquired EVM of the 64-QAM OFDM radio signal. The compatibility with fast RF carrier phase switching supports deployment scenarios involving mobile users at high velocity.

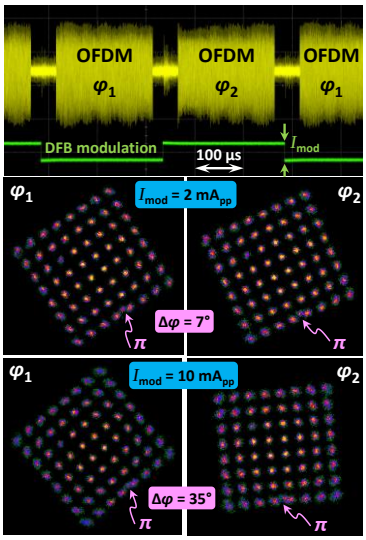

Fig. 5. Photonic RF carrier phase

Acknowledgement: This work was supported in part by the ERC under the EU Horizon-2020 programme (grant n° 804769).

6. References

[1] S.A. Busari et al., "Millimeter-Wave Massive MIMO Communication for Future Wireless Systems: A Survey," IEEE Comm. Surveys & Tutorials **20**, 836-869 (2018).

[2] X. Yi et al., "Photonic Beamforming Based on Programmable Phase Shifters With Amplitude and Phase Control," PTL **23**, 1286-1288 (2011).

[3] X. Wang et al., "Continuously tunable ultra-thin silicon waveguide optical delay line," Optica **4**, 507-515 (2017).

[4] D. Milovancev et al., "Analogue Coherent-Optical Mobile Fronthaul with Integrated Photonic Beamforming", JSAC **39**, 2827-2837 (2021).

[5] N.K. Srivastava et al., "Efficient Photonic Beamforming System Incorporating a Unique Featured Tunable Chirped Fiber Bragg Grating for Application Extended to the Ku-Band," IEEE Trans. Microw. Theory and Tech. **68**, 1851-1857 (2020).

[6] Y. Liu et al., "Ultra-Low-Loss Silicon Nitride Optical Beamforming Network for Wideband Wireless Applications," JSTQE **24**, 8300410, (2018).

[7] G. Wang et al., "Continuously tunable true-time delay lines based on a one-dimensional grating waveguide for beam steering in phased array antennas," Appl. Opt. **57**, 4998-5003 (2018).

[8] B.J. Vakoc et al., "A Tunable Dispersion Compensator Comprised of Cascaded Single-Cavity Etalons," PTL **17**, 1043-1045 (2005).